PERGAMON

International Journal of Solids and Structures 40 (2003) 649–670

INTERNATIONAL JOURNAL OF SOLIDS and STRUCTURES

www.elsevier.com/locate/ijsolstr

Asymptotic fields for dynamic crack growth in non-associative pressure sensitive materials

Xi Zhang [a], Qing-Hua Qin [b], Yiu-Wing Mai [b,c,*]

[a] *CSIRO, Division of Petroleum Resources, P.O. Box 3000, Glen Waverley, Vic. 3150, Australia*

[b] *Centre for Advanced Materials Technology (CAMT) and School of Aerospace, Mechanical and Mechatronic Engineering J07, The University of Sydney, Sydney, NSW 2006, Australia*

[c] *MEEM, City University of Hong Kong, 83 Tat Chee Avenue, Kowloon Tong, Hong Kong*

Received 4 March 2002; received in revised form 10 October 2002

Abstract

Asymptotic near-tip fields are analyzed for a plane strain Mode I crack propagating dynamically in non-associative elastic–plastic solids of the Drucker–Prager type with an isotropic linear strain hardening response. Eigen solutions are obtained over a range of material parameters and crack speeds, based on the assumption that asymptotic solutions are variable-separable and fully continuous. A limiting speed, beyond which a tendency to slope discontinuity in angular distributions of stresses and velocities is detected, is found to deviate from the associative models. At low strain-hardening rates, the onset of the plastic potential corner zone ahead of the crack-tip imposes another limit to the crack speed. Correspondingly, those limits imply the limits to the degree of non-associativity at a given crack speed. In addition, a tendency to slope discontinuity in the angular radial stress distribution sets another limit on the non-associativity at vanishing hardening rates.

Keywords: Crack-tip plasticity; Dynamic fracture; Non-associative plastic flow; Asymptotic analysis; Plane strain; Mode I crack

1. Introduction

Non-associative theories arise when the plastic potential surface that governs the plastic strain rate, does not coincide with the yield surface. In the presence of hydrostatic stress, there is plastic dilatation accompanying shear deformation in realistic materials due to the evolution of defects like voids, shear-bands and microcracks. These micro-defects facilitate the instability of macroscopic plastic flow such as necking between voids and intensive shear localization in void sheets. Non-associated flow rule was introduced by Mroz (1963) and Mandel (1966) to describe this mechanical behavior in geo-materials like rocks and soils. It is of interest in geo-mechanics within the context of hydraulic fracture (see Papanastasiou and Durban,

* Corresponding author. Address: Centre for Advanced Materials Technology (CAMT) and School of Aerospace, Mechanical and Mechatronic Engineering J07, The University of Sydney, Sydney, NSW 2006, Australia.

E-mail address: mai@aeromech.usyd.edu.au (Y.-W. Mai).

0020-7683/02/$ - see front matter
PII: S0020-7683(02)00616-9

2001). This important feature exists in more general porous materials such as sintered powder metals, polymeric materials and ceramics. In addition, it is anticipated that non-associated plastic flow applies to a broad range of material behavior at the later stage of material failure. For example, a physical model of polycrystalline metal plasticity based on the non-Schmid law implies the existence of vertices on the yield surface (see Kuroda and Tvergaard, 2001). The plastic flow in high strength steels, which although exhibit significantly less pressure sensitivity than granular materials, also follows a non-associated flow rule as reported experimentally by Spitzig et al. (1976). Tvergaard (1982) has studied the influence of void nucleation on ductile shear fracture at a free surface. The constitutive law used in his numerical computation obeys a non-associative flow rule due to the inclusion of void nucleation.

Investigations of the determination of asymptotic fields near a moving crack-tip play a dominant role on various aspects concerning the findings of fracture criteria and the stress and strain fields near the crack edge. This consideration was included by Amazigo and Hutchinson (1977) and Ponte-Castaneda (1987) for steady-state crack growth and by Achenbach et al. (1981) and Ostlund and Gudmundson (1988) for dynamic crack growth in elastic–plastic materials obeying the J_2 flow rule with isotropic linear strain-hardening. Plastic reloading on the crack flank was allowed by Ponte-Castaneda (1987) and Ostlund and Gudmundson (1988), so as to obtain reasonable results for low strain-hardening exponents. For pressure-sensitive materials following an isotropic yield condition and associated flow-rule, an asymptotic study was carried out by Li and Pan (1990) for stationary cracks, Bigoni and Radi (1993) for steady-state crack growth and Zhang and Mai (2000) for dynamic crack growth. It is found that the HRR-type field is still valid until the occurrence of a hydrostatic tension state ahead of the crack-tip. However, there were few studies concerning the effect of non-associativity except for the dynamic Mode III cracks by Lo and Peirce (1981) and quasi-static plane-stress Mode I cracks by Radi and Bigoni (1992).

Inertia effects on the crack-tip fields were studied by Gao and Nemat-Nasser (1983) and Leighton et al. (1987), among others. An important feature was the discontinuity in stress and strain fields for fast crack propagation in J_2-flow elastic–plastic materials at low strain-hardening rates, as noticed by Lam and Freund (1985) and Varias and Shih (1994). This was also addressed in the asymptotic analysis of Ostlund and Gudmundson (1988) by imposing a limit on the crack speed. Study on dynamic Mode I crack growth in perfectly plastic materials obeying the non-associated flow rule was performed by Nemat-Nasser and Obata (1990). The presence of a "stress jump" but not a "strain jump" was obtained in non-hardening plastic theories, even with an infinitesimal deviation from the normality. Brannon and Drugan (1993) performed a thermodynamic analysis of shock waves in non-classical materials and argued that discontinuous solutions (i.e., discontinuity of stress without a strain jump) could exist only with a sufficiently large non-normality degree. From these studies, effects of non-associativity are expected to be more evident at low strain-hardening. Nevertheless, it is necessary to obtain asymptotic results for very low hardening materials because the hardening ratio α of the tangent shear modulus G_t to the elastic shear modulus G is rather low in most cases. Usually this ratio is of the order of 10^{-4} for structural steels (Stahle, 1993). At low strain-hardening rates, the domain for asymptotic solutions must be sufficiently larger than the fracture zone so that asymptotic results can predict fracture resistance. The numerical solutions at very small hardening rates were presented by Ponte-Castaneda (1987) with an attempt to relate them to perfect plasticity. He found that there was a discontinuity in the velocity fields and the small α results could not be reduced to the corresponding perfectly-plastic fields. Moving cracks in very low hardening materials had been studied by Stahle (1993). He suggested that inertia might have a significant influence on the fracture process even at fairly low crack-tip speeds, especially on the occurrence of discontinuous stress rates. Here, we present a dynamic analysis of crack propagation in non-associative pressure sensitive solids to account for the coupled effects of crack speed and non-associativity on the fracture process.

The arrangement of the present paper is as follows. In Section 2, the constitutive equation with non-associated flow rule is reviewed and a statement of the problem is given. A set of governing equations for plane-strain Mode I crack growth are derived and the asymptotic expansions of stress and velocity fields

similar to those in Ponte-Castaneda (1987) and Ostlund and Gudmundson (1988) are employed. Next, in Section 3, numerical results are obtained for a range of material parameters to predict the influence of non-associativity and crack speed on the near-tip fields. Regarding small but not vanishing strain-hardening rates, the limiting solutions at low crack speeds and low non-associativity degrees are discussed in Section 4. A first-order approximation analysis based on the non-hardening solutions is carried out. Finally, the paper is concluded with a discussion on the near-tip fields, speed limit and maximum degree of non-normality in Section 5.

2. Basic equations and asymptotic methods

A simple small-strain incremental constitutive relation proposed by Rudnicki and Rice (1975) is used in which the normality is valid with regard to the flow potential g, but invalid for the yield function f. These two quantities are defined by:

$$\begin{aligned} f &= \tau_e + F(\sigma_{kk}) \\ g &= \tau_e + G(\sigma_{kk}) \end{aligned} \tag{1}$$

in which $\tau_e = \sqrt{s_{ij}s_{ij}/2}$, and $s_{ij} = \sigma_{ij} - \sigma_{kk}\delta_{ij}/3$. Functions F and G have the simple forms as $F(\sigma_{kk}) = \mu\sigma_{kk}/3$ and $G(\sigma_{kk}) = \beta\sigma_{kk}/3$. The two parameters, μ and β, reflect the level of pressure sensitivity with $\mu = \beta$ and the degree of non-normality $(\mu - \beta)$ with $\mu \neq \beta$. As measured in real materials, μ is always larger than β.

Applying the normal rule to g and the consistency condition to f, the following incremental stress–strain relations in the rate form can be obtained:

$$\dot{\boldsymbol{\varepsilon}} = \frac{1}{E}\left[(1+v)\dot{\boldsymbol{\sigma}} - v\,tr(\dot{\boldsymbol{\sigma}})\mathbf{I} + \frac{1}{h}\langle \mathbf{Q} : \dot{\boldsymbol{\sigma}}\rangle \mathbf{P}\right] \tag{2}$$

where v is Poisson's ratio, E elastic modulus, h hardening modulus divided by E and its value can be obtained by a bilinear strain-hardening model, as shown in Fig. 1, by: $1/(2(1+v)h) = (1/\alpha) - 1$ in which the hardening rate $\alpha = G_t/G$ (see Li and Pan, 1990 for more details). $\mathbf{I}$ is the second-order identity tensor. The symbol $\langle\ \rangle$ denotes the McAuley brackets and $\mathbf{P}$ and $\mathbf{Q}$ are the gradients of the flow potential and the yield surface in stress space, respectively:

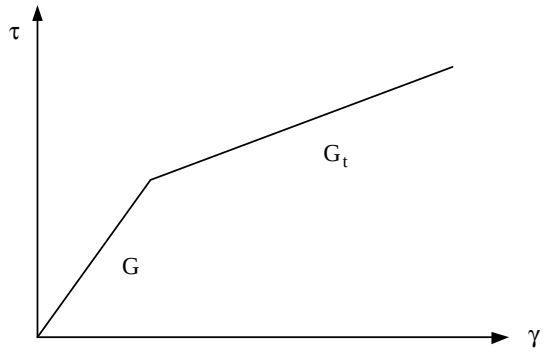

Fig. 1. Shear stress–strain curves in simple shear tests.

$$P_{ij} = \frac{\beta}{3}\delta_{ij} + \frac{\sqrt{3}}{2}\frac{s_{ij}}{\sigma_e}$$
$$Q_{ij} = \frac{\mu}{3}\delta_{ij} + \frac{\sqrt{3}}{2}\frac{s_{ij}}{\sigma_e} \tag{3}$$

where $\sigma_e = \sqrt{3}\tau_e$.

Consider a large body containing a straight extending crack. A Cartesian reference system is schematically illustrated in Fig. 2, with its origin located at the moving crack-tip. Following the formulation of the problem in Achenbach et al. (1981), all field variables are referred to the moving Cartesian coordinates (x_1, x_2, x_3) or cylindrical coordinates (r, θ, x_3). The deformation is assumed to be plane strain and the asymptotic near-tip fields in an approximate steady state. As established in Ostlund and Gudmundson (1988), the following identity that relates the material derivative to the spatial derivative along x_1, is adopted even for non-constant crack-tip speeds when $r \to 0$:

$$\dot{(\ )} = -V(\ )_{,1} = -V\left[\cos\theta(\ )_{,r} - \frac{\sin\theta}{r}(\ )_{,\theta}\right] \tag{4}$$

where V denotes the crack-tip velocity.

The relations between strain rates and deformation velocities can be written as:

$$\dot{\varepsilon}_{ij} = \frac{1}{2}(v_{i,j} + v_{j,i}) \tag{5}$$

where v_i are the two non-zero in-plane velocities and $v_3 = 0$ for plane strain case.

Referring to the cylindrical coordinates, the equations of motion become:

$$(r\sigma_{rr})_{,r} + \sigma_{r\theta,\theta} - \sigma_{\theta\theta} = \rho r\dot{v}_r$$
$$(r\sigma_{r\theta})_{,r} + \sigma_{\theta\theta,\theta} + \sigma_{r\theta} = \rho r\dot{v}_\theta \tag{6}$$

where ρ is the material density and the superposed dot denotes the material time derivatives. The following discussions on asymptotic solutions are based on the definition of a dimensionless parameter, $m_V = V/c_S$, in which $c_S = \sqrt{G/\rho}$ is the elastic shear wave speed.

The variable-separable asymptotic method holds because all basic equations are homogeneous in r. Similar to the procedure of Amazigo and Hutchinson (1977) and Ponte-Castaneda (1987), we have:

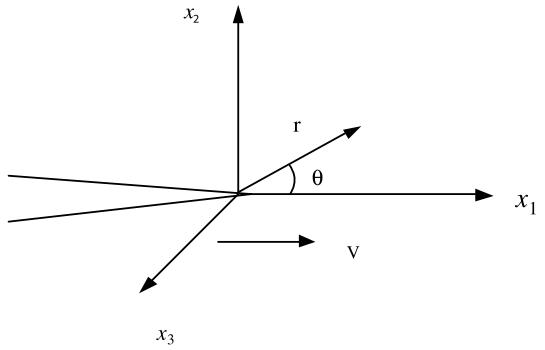

Fig. 2. The coordinates systems. Cartesian coordinates (x_1, x_2, x_3) and cylindrical coordinates (r, θ, x_3) are centered at the tip and move as the cracks grow.

$$v_\eta = \kappa(V/E)r^s/s\hat{v}_\eta(\theta)$$
$$\sigma_{ij} = \kappa r^s\hat{\sigma}_{ij}(\theta) \tag{7}$$

where s is a negative constant, referred to as the singularity level, κ is called the plastic stress intensity factor which is determined by the far field. Further, $\hat{v}_\eta$ and $\hat{\sigma}_{ij}$ in which $\eta = r, \theta$ and $i, j = r, \theta, 3$, are the angular functions of the velocities and stresses, respectively.

The critical condition for a particle ahead of the crack-tip experiencing unloading depends on the sign of the following plastic multiplier. Thus, elastic unloading occurs when:

$$Q_{ij}\dot{\sigma}_{ij} \leqslant 0 \tag{8}$$

Plastic reloading near the crack flanks has been allowed for in the asymptotic analyses of Ponte-Castaneda (1987) and Bigoni and Radi (1993). The secondary plastic zone occurs when the stress states of a particle in the wake reach the yield surface that is left at elastic unloading. For the non-associated materials with a yield surface in Eq. (1), the critical conditions for plastic reloading are:

$$Q_{ij}\dot{\sigma}_{ij} > 0 \quad \text{and} \quad \frac{\sigma_{ge}(\theta_2)}{\sin^s\theta_2} = \frac{\sigma_{ge}(\theta_1)}{\sin^s\theta_1} \tag{9}$$

in which $\sigma_{ge} = \sqrt{3}(\tau + \mu\sigma_{kk}/3)$; the angles θ_1 and θ_2 correspond to the angles of elastic unloading and plastic reloading, respectively.

It has been proven that for quasi-static crack growth in elastic–plastic materials that are stable in Drucker's sense, the continuities of stress and velocity are satisfied across the elastic–plastic boundary (see Narasimhan and Rosakis, 1987). This conclusion is questionable in the presence of material inertia and non-associativity. The continuous solutions cannot hold for all ranges of crack speeds and non-normality degrees. However, the full continuity of stress and velocity can be imposed on the interior boundaries so that the asymptotic analysis can be carried out. That is, the discontinuity is not assumed a priori and can be predicted from the asymptotic results. Therefore, both stress and velocity are continuous, giving:

$$\|\sigma_{ij}\| = \|v_i\| = 0 \tag{10}$$

where $\| \ \|$ denotes the jump of the quantitative across the elastic–plastic boundaries.

The general form of the governing equations by substituting Eq. (7) in Eqs. (2), (5) and (6) can be expressed as:

$$\mathbf{A}\frac{\mathrm{d}\mathbf{Y}}{\mathrm{d}\theta} = \mathbf{B} \tag{11}$$

where the matrices $\mathbf{A}$ and $\mathbf{B}$ are functions of material parameters and crack-tip speed,

$$\mathbf{Y} = \{y_i, i = 1, 6\} = \{\hat{v}_r, \hat{v}_\theta, \hat{\sigma}_{r\theta}, \hat{\sigma}_{rr}, \hat{\sigma}_{\theta\theta}, \hat{\sigma}_{33}\}^{\mathrm{T}}$$

and

$$\frac{\mathrm{d}\mathbf{Y}}{\mathrm{d}\theta} = \left\{\frac{y_1'}{2}, y_2', \dot{\tilde{\sigma}}_{r\theta}, \dot{\tilde{\sigma}}_{rr}, \dot{\tilde{\sigma}}_{\theta\theta}, \dot{\tilde{\sigma}}_{33}\right\}^{\mathrm{T}}$$

in which the prime denotes the derivative to the angle $\boldsymbol{\theta}$ and $\dot{\tilde{\sigma}}_{ij} = \dot{\sigma}_{ij}/(EVr^{s-1})$. The special forms of these matrices are listed in Appendix A.

Mode-I symmetry at $\theta = 0$ requires:

$$y_1'(0) = y_2(0) = y_3(0) = y_4'(0) = y_5'(0) = y_6'(0) = 0 \tag{12}$$

While on the crack surface, tractions $\sigma_{\theta\theta}$ and $\sigma_{r\theta}$ vanish. Hence:

$$y_3(\pi) = y_5(\pi) = 0 \tag{13}$$

Continuity of all fields requires no jump across the elastic–plastic boundaries, that is:

$$\|y_i\| = 0 \tag{14}$$

Furthermore, the normalization condition must be introduced so that all initial values of y_i are specified at $\theta = 0$. Thus:

$$y_5(0) = 1 \tag{15}$$

The above system of first-order ordinary differential equations can be solved by the standard Runge–Kutta method and the Newton–Raphson iteration scheme, as discussed by Press et al. (1992). The initial values of s and $y_4(0)$ are assigned tentatively. The integration is performed and the values $y_3(\pi)$ and $y_5(\pi)$ are checked. Based on errors for $y_3(\pi)$ and $y_5(\pi)$, initial values of s and $y_4(0)$ are reassigned by the iterative scheme. Numerical results reported in Section 3 have been obtained by using a double precision program with a relative error in each step less than 10^{-7}. Since the matrix **A** in Eq. (11) is singular at $\theta = 0$, the restriction condition $y_4'(\theta) = y_6'(\theta) = 0$ is imposed on a very small angle ($\theta < 10^{-6}$).

3. Numerical results

3.1. Singularity

Tables 1–3 provide values of s, θ_1 and θ_2 for $v = 1/3$ at various crack-tip speeds and material parameters (α, μ, β). As expected, the results are recovered for all associative models in Ostlund and Gudmundson (1988), Bigoni and Radi (1993) and Zhang and Mai (2000). The value of $|s|$ is higher at $\alpha = 0.1$ than at $\alpha = 0.001$. A small but non-vanishing value of $|s|$ can be found at $\alpha = 0.0001$ An increase in μ can reduce $|s|$ if the associated flow rule is applied to the plastic deformation. However, the stress singularity level increases with the non-normality degree $(\mu - \beta)$. It is interesting to note that non-associativity can enhance the singularity level, compared with the associative flow rule. The higher singularity level obtained in the presence of non-associativity provides a more reasonable explanation for the lower fracture toughness of porous materials (see Wei, 2000).

Table 1
Numerical results of s and $y_{4(0)}$, unloading and reloading angles (θ_1 and θ_2) under plane strain condition ($\alpha = 0.1$)

μ	β	m_V	M_V	s	$y_{4(0)}$	θ_1	θ_2
0.0	0.0	0.000	0.000	−0.20957	1.09033	122.21	175.31
		0.100	0.316	−0.20346	1.09137	120.65	175.76
		0.200	0.632	−0.18137	1.09242	115.43	177.19
		0.300	0.948	−0.10924	1.07362	101.36	179.95
0.1	0.0	0.000	0.000	−0.229228	1.06336	107.84	179.69
		0.100	0.316	−0.223743	1.06596	106.73	179.74
		0.200	0.632	−0.203838	1.07292	102.78	179.86
		0.300	0.948	−0.141278	1.07628	94.00	179.99
		0.315	0.992	−0.105205	1.06916	90.66	180.00
	0.1	0.000	0.000	−0.20179	1.01200	107.60	179.88
		0.100	0.316	−0.19657	1.01569	106.47	179.92
		0.200	0.632	−0.17743	1.02667	102.65	179.98
		0.300	0.948	−0.11179	1.04441	95.94	180.00

Table 2
Numerical results of s and $y_{4(0)}$, unloading and reloading angles (θ_1 and θ_2) under plane strain condition ($\alpha = 0.001$)

μ	β	m_V	M_V	s	$y_{4(0)}$	θ_1	θ_2
0.0	0.00	0.000	0.000	−0.05641	0.75381	137.02	138.52
		0.010	0.316	−0.05237	0.75149	136.83	138.47
		0.020	0.632	−0.03977	0.74385	136.09	138.62
0.1	0.00	0.000	0.000	−0.09239	0.90987	136.74	138.50
		0.010	0.316	−0.08770	0.90500	136.48	138.34
		0.020	0.632	−0.07300	0.88948	135.68	137.82
	0.10	0.000	0.000	−0.05369	0.82810	133.88	135.56
		0.010	0.316	−0.04999	0.82500	133.65	135.54
		0.020	0.632	−0.03837	0.81480	132.96	135.81
0.2	0.15	0.000	0.000	−0.06736	0.94208	131.79	133.67
		0.010	0.316	−0.06371	0.93662	131.57	133.63
		0.020	0.632	−0.05219	0.91976	130.85	133.55
	0.20	0.000	0.000	−0.05003	0.89696	130.63	132.56
		0.010	0.316	−0.04677	0.89298	130.44	132.67
		0.020	0.632	−0.03647	0.88006	129.70	133.13
0.3	0.300	0.0000	0.000	−0.04562	0.96371	127.18	129.84
		0.0100	0.316	−0.04288	0.95790	126.98	129.95
		0.0200	0.632	−0.03412	0.94062	126.30	130.59
		0.0300	0.948	−0.01544	0.90558	123.58	135.19
		0.0320	1.024	−0.00523	0.89181	114.55	151.15
	0.279	0.0000	0.000	−0.05188	0.99725	127.51	130.05
		0.0100	0.316	−0.04926	0.98493	127.33	130.10
		0.0200	0.632	−0.04026	0.96097	126.68	130.49
		0.0300	0.948	−0.02127	0.92192	124.85	132.97
		0.0313	0.989	−0.01667	0.91272	124.03	134.55
	0.270	0.0130	0.411	−0.04975	0.99646	127.37	130.27
		0.0250	0.790	−0.03511	0.95326	126.33	130.95
		0.0300	0.948	−0.02366	0.92924	125.25	132.42
		0.0309	0.976	−0.02070	0.92314	124.85	133.08
	0.250	0.0220	0.695	−0.04534	0.99607	131.52	130.65
		0.0280	0.885	−0.03411	0.95920	126.42	131.17
		0.0300	0.948	−0.02879	0.94684	160.39	131.66
	0.230	0.0270	0.853	−0.04131	0.99755	127.08	130.97
		0.0280	0.885	−0.03910	0.98527	126.96	131.03
		0.0290	0.916	−0.03656	0.97620	126.79	131.14

With increasing crack speed, $|s|$ decreases when all material parameters are fixed. The same trend can be found in elastic–plastic materials obeying the J_2-flow rule. There is no unified relation as $s \approx -\alpha^{1/2}$ in Achenbach et al. (1981) and Ponte-Castaneda (1987), due to the combinations of μ, β and m_V. At the upper-limit crack speeds, $s \to -\alpha$ for $\alpha = 0.1$, while $s \to -\alpha^{1/2}$ for $\alpha = 0.0001$, as shown in Tables 1 and 3. Fig. 3 shows the combined effects of material inertia and non-associativity on the singularity level at $\alpha = 0.001$. It is evident that the results in the presence of non-associativity deviate from those obtained for associative models.

Table 3
Numerical results of s and $y_{4(0)}$, unloading and reloading angles (θ_1 and θ_2) under plane strain condition ($\alpha = 0.0001$ and $\mu = 0.1$)

β	m_V	M_V	s	$y_{4(0)}$	θ_1	θ_2
0.100	0.0000	0.000	−0.050963	0.82324	134.33	134.82
0.080	0.0000	0.000	−0.058893	0.83711	134.93	135.39
0.075	0.0000	0.000	−0.060903	0.84082	135.09	135.55
0.072	0.0000	0.000	−0.062118	0.84311	135.18	135.66
0.070	0.0010	0.100	−0.063956	0.84956	136.54	137.51
0.070	0.0050	0.500	−0.053558	0.83867	135.82	136.82
0.065	0.0050	0.500	−0.055489	0.84262	136.04	137.02
0.080	0.0075	0.750	−0.035723	0.81531	134.39	135.43
0.070	0.0075	0.750	−0.039324	0.82289	134.83	135.89
0.060	0.0075	0.750	−0.042849	0.83039	135.19	136.23
0.080	0.0050	0.500	−0.048804	0.82748	134.44	134.95
0.080	0.0070	0.700	−0.038580	0.81696	133.93	134.50
0.080	0.0090	0.900	−0.023337	0.79893	133.16	133.90
0.080	0.00950	0.950	−0.018093	0.79159	132.86	133.76
0.080	0.009588	0.959	−0.017039	0.78998	132.81	133.72

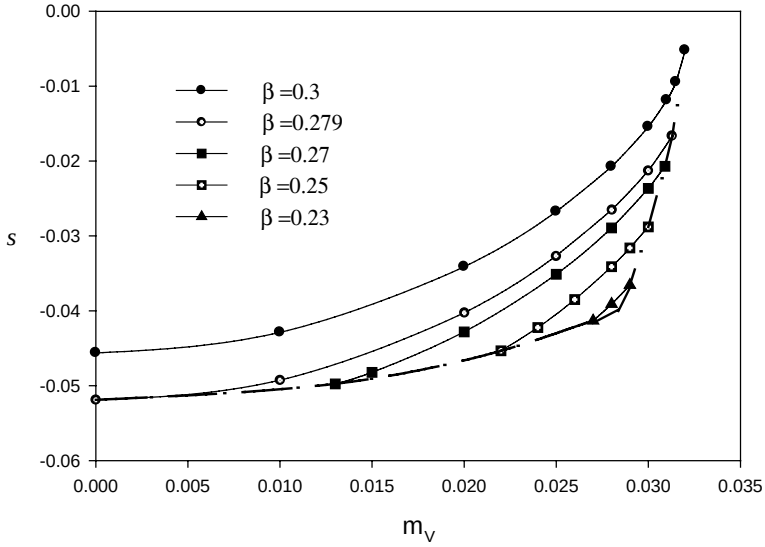

Fig. 3. Variations of s with crack speed and non-normality degree for $\alpha = 0.001$ and $\mu = 0.3$.

3.2. Crack speeds and material parameters

As discussed by Li and Pan (1990), Bigoni and Radi (1993) and Zhang and Mai (2000), a hydrostatic state of stress ahead of the crack-tip occurs for associative materials, when μ attains a limiting value. The singular behavior of plastic potential does not cause a change in the characteristics of the equations. This feature is also found here when the effects of inertia and non-associativity are included. For example, $y_4(0)$ approaches unity when μ reaches its limit for pressure-sensitive materials, and it also approaches unity at

non-zero crack speed and with a deviation from normality, as shown in Table 2. From Fig. 3, this singular behavior provides an estimate of the minimum crack speed $m_V^{\min}$ at specified material parameters. However, as found by Ostlund and Gudmundson (1988), there is a maximum crack speed $m_V^{\max}$ due to the loss of ellipticity of the governing equations. More details will be given later in this section. Different to previous studies, the limit depends not only on the hardening rate, but also on the degree of non-associativity as shown in Fig. 3. The dashed curve in this figure provides the envelope for the crack-tip speeds at a specified strain-hardening exponent.

With increasing degree of non-associativity, the loss of strong ellipticity is possible only for vanishing strain hardening rates. In this case, the occurrence of a hydrostatic state of stress ahead of the tip can be ruled out from the results listed in Table 3. We will deal with this case in Section 4. It is found in Tables 1–3 that the range of $(\mu - \beta)$ decreases at low α or high μ when the inertia effect is not included. For example, $(\mu - \beta)$ at $\mu = 0.1$ can reach as high as 0.1 for $\alpha = 0.1$ and 0.001, but it is 0.028 for $\alpha = 0.0001$. Moreover, it is just 0.021 for $\alpha = 0.001$ and $\mu = 0.3$, compared with 0.028 for $\alpha = 0.0001$ and $\mu = 0.1$. In addition, the inertia effect can extend the range of degree of non-normality. It is evident in Fig. 3 and Table 2 that the limit of $(\mu - \beta)$ can be increased from 0.021 at quasi-static crack growth to more than 0.07 for $\alpha = 0.001$ and $\mu = 0.3$ at $m_V = 0.029$.

3.3. Unloading sectors

As in classical elastic–plastic materials, a three-sector division around the tip is obtained at low hardening rates $\alpha \leqslant 0.1$. The range of elastic unloading sectors becomes narrower at a low hardening rate $\alpha = 0.001$, compared with that at $\alpha = 0.1$. An increase in crack speed can expand the unloading sectors in the presence of non-associativity. However, at a given crack speed, non-associativity will reduce the angular range of unloading sectors.

3.4. Stress states

The plots of angular distributions of stress components are given in Figs. 4–6 for various crack speeds for the case of $\alpha = 0.1$, $\mu = 0.1$ and $\beta = 0$. $m_V^{\max}$ is close to 0.315 beyond which no asymptotic solutions can be obtained. When $m_V \leqslant 0.2$, there is no clear variation in stress with crack speed. Some features for associative models are recovered, for instance, a compressive radial stress on the crack flank. When $m_V > 0.2$, the variation in shear stresses is recognizable with increasing crack speed, Fig. 4. At crack speed higher than 0.315, drastic changes in angular distributions of stresses are observed around $\theta = \pi/2$ from the crack-line. Therefore, a tendency to form a "jump" in the slopes of stress components is anticipated around $\theta = \pi/2$.

3.5. Velocity fields

A change in crack speeds can produce clear variations in velocity fields around the crack-tip, Fig. 7. The larger the crack speed, the smaller the plastic strain ahead of the crack-tip due to reductions in the slope of the hoop velocity, the magnitude of radial velocity, and the stress singularity. Thus, fast crack propagation can induce spontaneous brittle cracking caused by the confinement of plastic deformation. Conversely, when m_V approach 0.315, the variation in $\hat{v}_r$ becomes dramatic in a narrow range near $\theta = \pi/2$, Fig. 7. It is expected from Figs. 4 and 7 that as the crack growth rate increases to the upper limit, there is a tendency to slope discontinuity in the velocity fields for non-associative models. This finding is also addressed in the finite-element results of quasi-static crack growth by Lam and Freund (1985) using J_2-flow theory and by Varias and Shih (1994) using deformation theory. It is interesting to note that the "strain jump" is confined to a region near $\theta = \pi/2$, as obtained numerically by Varias and Shih (1994).

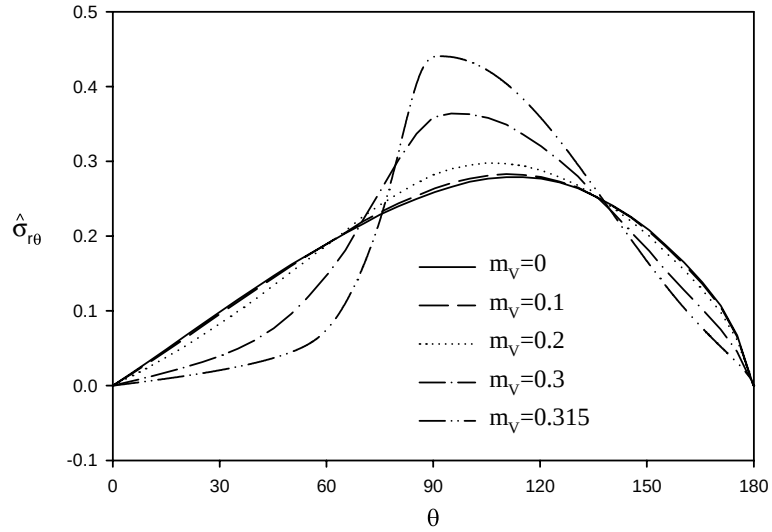

Fig. 4. Angular distributions of shear stress $\hat{\sigma}_{r\theta}$ at various crack speeds for $\alpha = 0.1$, $\mu = 0.1$ and $\beta = 0.0$.

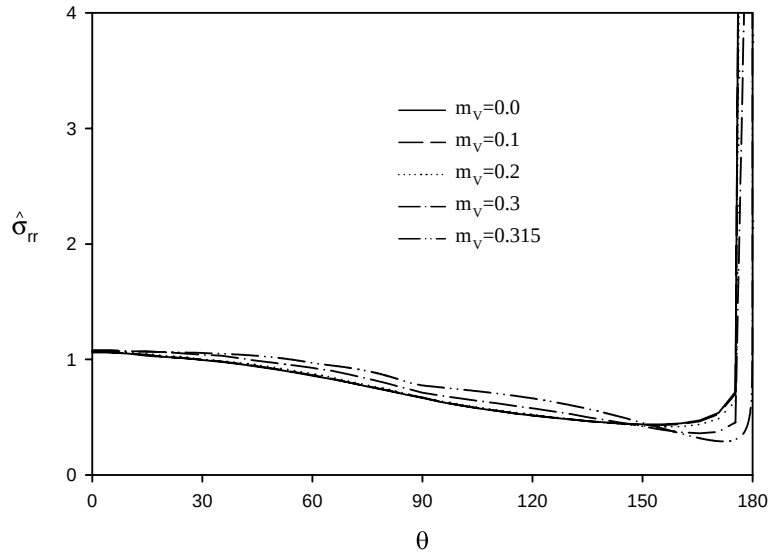

Fig. 5. Angular distributions of shear stress $\hat{\sigma}_{r\theta}$ at various crack speeds for $\alpha = 0.1$, $\mu = 0.1$ and $\beta = 0.0$.

3.6. The upper speed limit at medium strain hardening

For convenience, the relative crack speed is redefined as $M_V = V/C_S$ in which $C_S = \sqrt{G_t/\rho}$ is the plastic shear wave speed and its upper limit is denoted as M_V^L. In our calculations, $M_V^L \to 1$ as indicated in Tables 1 and 2. But it is slightly influenced by the choices of μ and β, especially at low strain-hardening rates, as

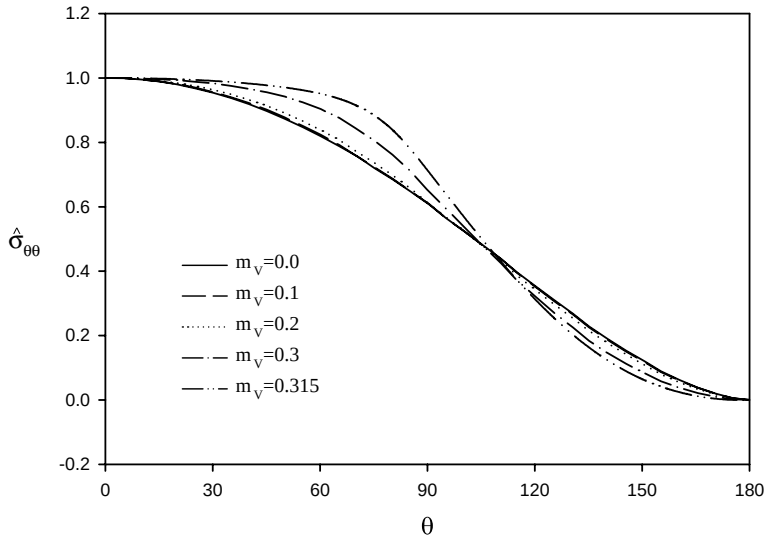

Fig. 6. Angular distributions of shear stress $\hat{\sigma}_{\theta\theta}$ at various crack speeds for $\alpha = 0.1$, $\mu = 0.1$ and $\beta = 0.0$.

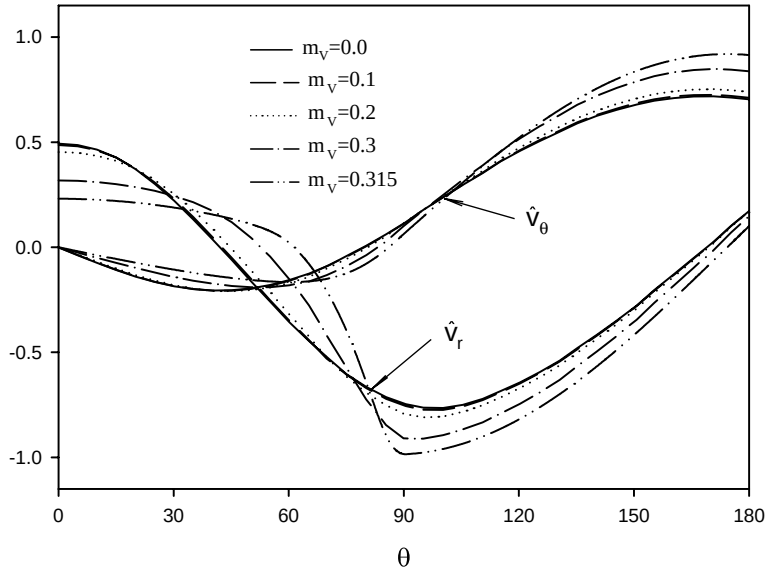

Fig. 7. Angular distributions of velocity fields $\hat{v}_i$ at various crack speeds for $\alpha = 0.1$, $\mu = 0.1$.

given in Table 2. For instance, at $\alpha = 0.001$, M_V^L is 1.024 for $\mu = \beta = 0.3$ and 0.916 for $\mu = 0.3$ and $\beta = 0.23$. This reduction in M_V^L is also detectable in Fig. 3.

Due to the complexity of the problem, much attention is focused on high and medium strain-hardening rates, that is, α does not approach zero. We deal with the case of $\alpha = 0.1$ for simplicity. It is found from Table 1 that the maximum value of $(\mu - \beta)$ can be of the order of α. Based on first-order approximation to

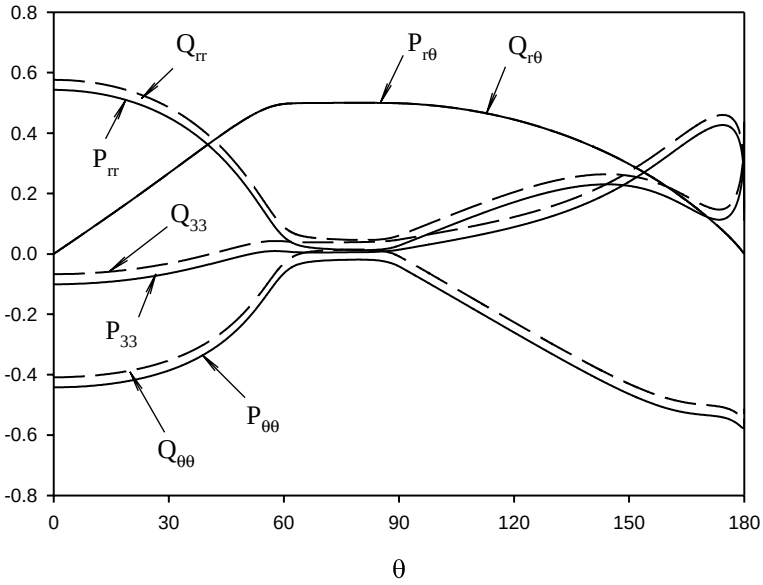

Fig. 8. Angular distributions of P_{ij} and Q_{ij} at maximum crack speed $m_v = 0.315$ for $\alpha = 0.1$, $\mu = 0.1$ and $\beta = 0$.

the numerical results in Table 1, it is reasonable to assume that $s = \mathrm{O}(-\alpha)$ and $\mu - \beta = \mathrm{O}(\alpha)$ at $\alpha = 0.1$. As stated above, the speed limit is determined by the stress state near $\theta = \pi/2$. There is, a small region around $\theta = \pi/2$ in which $P_{r\theta} = Q_{r\theta} \approx 1/2$, and other components of the tensors **P** and **Q** are less than one-tenth of this value as illustrated in Fig. 8 for $\mu = 0.1$ and $\beta = 0.0$.

Referring to the coefficients of the system of ODEs listed in Appendix A, the following expression can be obtained for the angular functions of stress rates:

$$\begin{aligned} \dot{\tilde{\sigma}}_{r\theta} &= -b_1 + a_{11} y_1'/2 \\ \dot{\tilde{\sigma}}_{\theta\theta} &= -b_2 + a_{22} y_2' \end{aligned} \tag{16}$$

and

$$\begin{aligned} \dot{\tilde{\sigma}}_{rr} &= c_4 - c_{41} a_{11} y_1'/2 - c_{42} a_{22} y_2' \\ \dot{\tilde{\sigma}}_{33} &= c_6 - c_{61} a_{11} y_1'/2 - c_{62} a_{22} y_2' \end{aligned} \tag{17}$$

in which, c_4 and c_6 are continuous functions of θ. $c_{41} = (a_{43}a_{66} - a_{46}a_{63})/D_1$, $c_{42} = (a_{45}a_{66} - a_{46}a_{65})/D_1$, $c_{61} = (a_{63}a_{44} - a_{64}a_{65})/D_1$ and $c_{62} = (a_{65}a_{44} - a_{64}a_{45})/D_1$, and $D_1 = a_{44}a_{66} - a_{64}a_{46}$.

Inserting Eqs. (16) and (17) into Eq. (11), the governing equations for the velocities are:

$$\begin{aligned} d_{11} y_1'/2 + d_{12} y_2' &= e_1 \\ d_{21} y_1'/2 + d_{22} y_2' &= e_2 \end{aligned} \tag{18}$$

in which e_1 and e_2 are continuous functions of θ,

$$\begin{aligned} d_{11} &= a_{31} + a_{11}(a_{33} - c_{41}a_{34} - c_{61}a_{36}), \quad d_{12} = a_{22}(-c_{42}a_{34} - c_{62}a_{36} + a_{35}), \\ d_{21} &= a_{11}(-c_{41}a_{54} - c_{61}a_{56} + a_{53}), \quad d_{22} = a_{52} + a_{22}(a_{55} - c_{42}a_{54} - c_{62}a_{56}) \end{aligned}$$

Considering the first-order approximation of P_{ij} and Q_{ij}, it is found that the value of D_1 defined in Eq. (17) does not approach zero. In the case of $\mu = 0.1$ and $\beta = 0.0$, D_1 approaches unity. Substituting

small values of P_{rr}, Q_{rr}, $P_{\theta\theta}$ and $Q_{\theta\theta}$ in the coefficients a_{ij} listed in Appendix A, it is found that $a_{33} \to s/2h \gg a_{34}$, a_{35}, a_{36} and $a_{55} \to s \gg a_{53}$, a_{54}, a_{56}. However, c_{41}, c_{42}, c_{61}, $c_{62} \to 1$. The determinant of the coefficient matrix in Eq. (18), $D_2 = d_{11}d_{22} - d_{12}d_{21}$, gives:

$$D_2 = (a_{31} + a_{11}a_{33})(a_{52} + a_{22}a_{55}) - a_{11}a_{53}a_{22}a_{35} \approx 1 - a_{11}a_{33} = 1 - m_V^2 \sin^2\theta/\alpha = 1 - M_V^2 \sin^2\theta \qquad (19)$$

It should be noted the facts that $a_{33} \gg a_{55}$ and $a_{11} = 2a_{22}$ are invoked in the above derivation.

D_2 approaches zero by increasing the crack speed. This results in the loss of a fully continuous power-singularity near-tip field as required. At $\theta \to \pi/2$, the critical condition $D_2 = 0$ leads to a conclusion that M_V^L must be less than unity for continuous solutions.

4. The hardening limit

Motivated by the work of Stahle (1993), we examine the solutions for small α's for non-associative solids in this section. It is found in Table 3 that the ranges of crack speed and non-normality degree become narrow compared with the results at $\alpha = 0.1$. In Table 3, s can be at least of the order of $-\alpha^{1/2}$ and does not approach zero in the same order as α, even though it tends to zero when the strain-hardening rate vanishes. An increase in $(\mu - \beta)$ can enhance the stress singularity, as it does at large α's. However, the crack speed can produce evident changes in s at very low hardening rates. Table 3 shows that when M_V approaches unity, the value of s is reduced to 0.017039, less than one-third of that for quasi-static crack growth. Thus when material inertia is included, an infinitesimal speed can affect the solutions.

The range of $(\mu - \beta)$ is less than 0.03, much less than 0.1 for $\alpha = 0.1$. This means that the degree of non-normality allowed is much reduced at vanishing hardening rates. The thermodynamic analysis of Brannon and Drugan (1993) showed that the stress jump is possible only for a sufficiently large deviation from normality. However, the results provided here indicate a limit to the non-normality degree. From Table 3, we found that this limit is not caused by the singular behavior of the plastic potential because the stress state ahead of the crack-tip is not in tension. We will discuss the reason later.

A small angular region of elastic unloading must be introduced for quasi-static crack growth in perfectly plastic materials as pointed out by Rice (1982). This feature is recovered in Table 3 for dynamic crack growth, although the range of unloading sectors is very narrow. The angular range of the elastic unloading region is less than 0.92° at $\alpha = 0.0001$ for all combinations of crack speeds and material parameters.

Angular distributions of stress components at two different crack speeds for $\alpha = 0.0001$ are plotted in Fig. 9 for the case of $\mu = 0.1$ and $\beta = 0.08$. It is found that there is little difference in $\hat{\sigma}_{\theta\theta}$ and $\hat{\sigma}_{r\theta}$, but a visible change in $\hat{\sigma}_{rr}$ caused by an increase in crack speed. As given in Appendix B, the plastic sectors around the crack-tip in the perfectly plastic materials obeying the non-associated flow-rule can also be roughly classified into two types; a constant stress sector and a center fan, when $(\mu - \beta)$ is very small. The requirement on small magnitudes of material parameters μ and β at vanishing α seems reasonable as indicated in Table 3. Shown in Fig. 9, the small-α solutions near $\theta = \pi/2$ are similar to the center fan solution in that $\hat{\sigma}_{rr} = \hat{\sigma}_{\theta\theta}$. Therefore, a first-order approximation to the corresponding solutions for quasi-static crack growth in perfectly plastic materials can be assigned to the stress distribution near $\theta = \pi/2$. However, it is noted that the introduction of an elastic-unloading region makes the stress distribution different from the stationary cracks.

In the singular center fan, $Q_{rr} \approx -(\mu - \beta)/6$ obtained from Appendix B for perfectly plastic materials on the basis of $P_{33} = 0$ and $Q_{33} = (\mu - \beta)/3$. Hence, $P_{rr} \approx (\mu - \beta)/2$. Considering $Q_{ii} = \mu$ and $P_{ii} = \beta$, we have $P_{\theta\theta}$ and $Q_{\theta\theta} \to \mu$ and β, respectively, if the non-normality degree is not too large.

In particular, the speed limit M_V^L is less than unity due to the effect of non-associativity, as shown in Table 3. Substitution of the components of $\mathbf{P}$ and $\mathbf{Q}$ in the expression of σ_e yields $P_{r\theta} \approx Q_{r\theta} \approx 1/2$. Finally, the coefficients in Eq. (11) are given by:

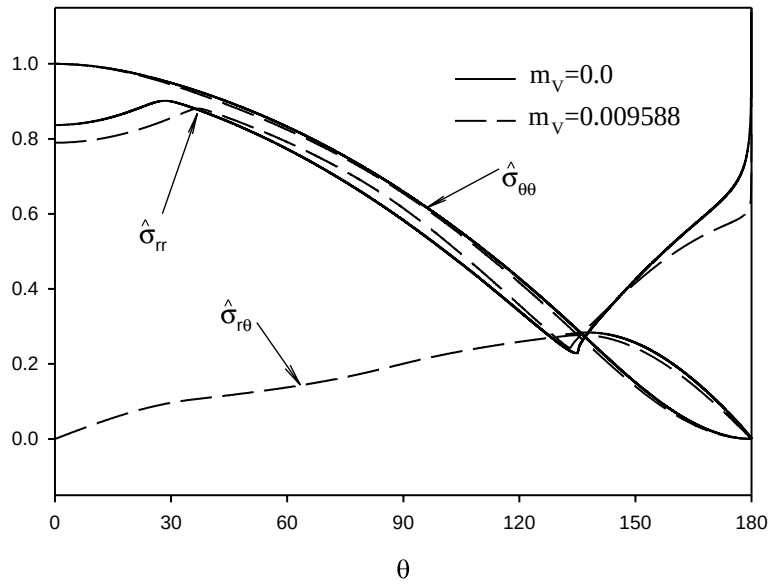

Fig. 9. Angular distributions of stress components $\hat{\sigma}_{ij}$ at two crack speeds for $\alpha = 0.0001$, $\mu = 0.1$ and $\beta = 0.08$.

$$\begin{aligned} &a_{33} \to s/2h \quad a_{34} \to sQ_{rr}/2h \quad a_{35} \to s\mu/2h \quad a_{36} \to sQ_{33}/2h \\ &a_{43} \to P_{rr}/h \quad a_{44} \to Q_{rr}P_{rr}/h \quad a_{45} \to \mu P_{rr}/h \quad a_{46} \to (\mu-\beta)P_{rr}/3h \\ &a_{53} \to sP_{\theta\theta}/h \quad a_{54} \to sQ_{rr}P_{\theta\theta}/h \quad a_{55} \to s\mu P_{\theta\theta}/h \quad a_{56} \to (\mu-\beta)P_{\theta\theta}/3h \\ &a_{63} \to 0 \quad a_{64} \to -v \quad a_{65} \to -v \quad a_{66} \to 1 \end{aligned} \tag{20}$$

since $s \to \mathrm{O}(-\alpha^{1/2})$ at vanishing hardening rates.

The coefficients in Eq. (17) can be obtained as follows:

$$\begin{aligned} &c_{41} = P_{rr}/D_1 h \quad c_{42} = \mu P_{rr}/D_1 h \\ &c_{61} = vP_{rr}/D_1 h \quad c_{62} = v\mu P_{rr}/D_1 h \end{aligned} \tag{21}$$

in which $D_1 = 1 - v^2 + P_{rr}Q_{rr}/h + vP_{rr}Q_{33}/h$.

All the values listed in Eqs. (20) and (21) are inserted into the coefficients in Eq. (18). Thus $d_{11} \to -1 + a_{11}s[1 + P_{rr}(Q_{rr} + vQ_{33})/D_1 h]/2h$, $d_{12} \to a_{22} \times \mathrm{O}(1)$, $d_{21} \to a_{11} \times \mathrm{O}(1)$ and $d_{22} \to -1 + a_{22}s\mu(\mu+\beta)/2h$. If $\mu \approx o(1)$, it gives

$$D_2 \to 1 - a_{11}s\Lambda/2h = 1 - \Lambda M_v^2 \sin^2\theta \tag{22}$$

in which $\Lambda = 1 + P_{rr}(Q_{rr} + vQ_{33})/D_1 h$.

Angular distributions of D_2 are given in Fig. 10 for different crack speeds at $\alpha = 0.0001$, $\mu = 0.1$ and $\beta = 0.08$. Near $\theta = \pi/2$, $Q_{rr} \approx -0.0025 = -(\mu-\beta)/8$ at $m_V = 0.009588$ is shown in Fig. 11. Higher speeds than 0.009588 cannot be obtained in the calculations. The small value of Q_{rr} confirms our assumption that the stress states can be approximated by the center-fan solutions in the non-hardening cases. Substitution of $D_1 = 0.9568$ and Q_{rr}, Q_{33} in Eq. (22) yields

$$D_2 = 1 - [1 + 11(\mu-\beta)^2/1728hD_1]M_V^2 \sin^2\theta = 1 - 1.071M_V^2 \sin^2\theta$$

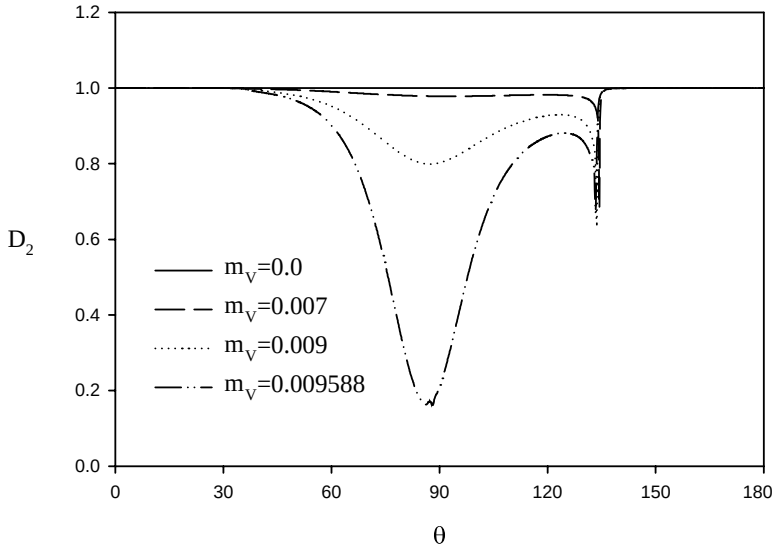

Fig. 10. Angular distributions of D_2 at different crack speeds for $\alpha = 0.0001$, $\mu = 0.1$ and $\beta = 0.08$ showing the tendency for vanishing D_2 is evident near the speed limit.

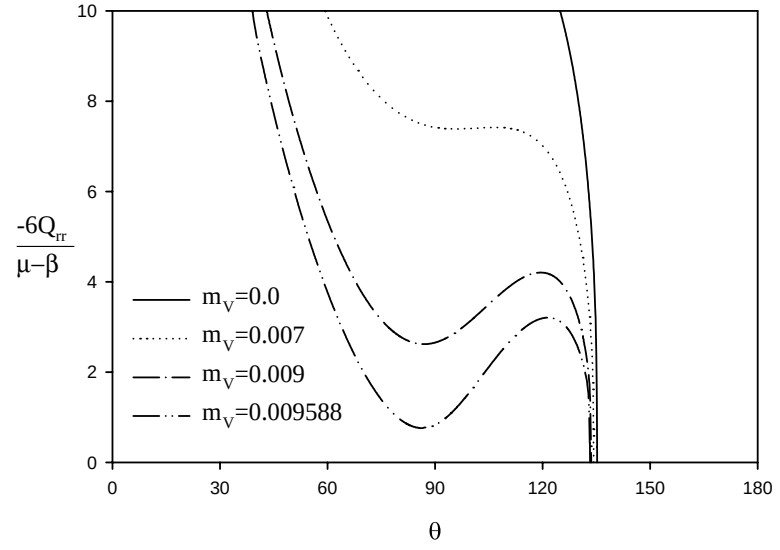

Fig. 11. Angular distributions of Q_{rr} at various crack speeds for $\alpha = 0.0001$, $\mu = 0.1$ and $\beta = 0.08$.

Thus M_V^L is 0.9663 as $D_2 = 0$. It is close to our prediction, $M_V^L = 0.9588$ in Table 3. It should be noted that the condition of $\mu = O(1)$ is required in the derivation of Eq. (22).

Now we obtain the maximum value of $(\mu - \beta)$ as $\alpha \to 0$. Because $M_V < 1$ and $s \approx O(-\alpha^{1/2})$, the coefficients a_{11} and a_{22} in Eq. (11) are at most of the order of $O(\alpha^{1/2})$. As shown in Fig. 12, there are no dramatic changes in $\hat{\sigma}_{r\theta}$ and $\hat{\sigma}_{\theta\theta}$ by varying the degree of non-normality at $M_V = 0$ An important feature is the rapid variation of the radial stress $\hat{\sigma}_{rr}$ near the elastic–plastic boundary in the secondary plastic zone. The slope of the radial stress $\hat{\sigma}_{rr}$ becomes steeper with increasing non-normality degree. This implies that $\sigma'_{rr} \gg 1$ since

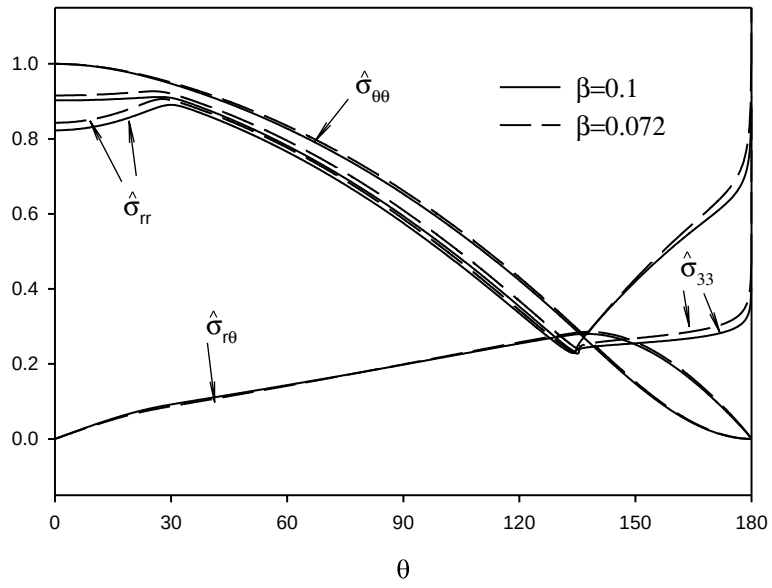

Fig. 12. Angular distributions of stress components $\hat{\sigma}_{ij}$ at different values of β for $\alpha = 0.0001$, $\mu = 0.1$ and $m_V = 0$.

the stress rate is expressed by Eq. (4). It also means that D_1 approaches zero at a finite value of $(\mu - \beta)$ and $M_V = 0$.

Since no jump is permitted in stresses and Q_{ij} a priori, $Q_{ij}\hat{\sigma}'_{ij}$ should be a continuous function of the angle prior to the presence of stress jump. When approaching the elastic–plastic boundary, $Q_{ij}\hat{\sigma}'_{ij} = 0$ according to (B.6) in Appendix B. From Fig. 12, it is found that in the secondary plastic zone, $\sigma'_{rr} \to \infty$ at the points adjacent to the elastic–plastic boundary, thus $Q_{rr} \to 0$. Hence, $P_{rr} \to -(\mu - \beta)/3$. But, $Q_{33} = (\mu - \beta)/3$ due to plane-strain conditions. Substituting these relations in the expression of D_1 yields:

$$D_1 = a_{44}a_{66} - a_{46}a_{64} = 1 - v^2 + \frac{v}{h}P_{rr}Q_{33} = 1 - v^2 - \frac{v}{9h}(\mu - \beta)^2 \tag{23}$$

Hence it yields the range of $(\mu - \beta)$ at a given small hardening rate. That is,

$$\mu - \beta < \sqrt{\frac{9h(1 - v^2)}{v}} \approx \sqrt{\frac{9\alpha(1 - v)}{2v}} \tag{24}$$

The numerical results of $D_1(\theta)/D_1(0)$ from various combinations of material parameters are shown in Fig. 13(a) in which $D_1(0)$ depends significantly on α. The elastic unloading zone is highlighted by the results on the x-axis magnified in Fig. 13(b). It is found that D_1 becomes very small at the points adjacent to elastic–plastic boundary in the secondary plastic zone when $\mu - \beta = 0.028$. When $v = 1/3$ and $\alpha = 0.0001$, we have $(\mu - \beta) < 0.03$ from Eq. (24). It is in a good agreement with the numerical results in Table 3, where the maximum value of $(\mu - \beta)$ is 0.028. This result further confirms that the range of non-normality depends on the strain-hardening exponent. An infinitesimal value of $(\mu - \beta)$ that is of the order of $O(\alpha^{1/2})$ would lead to the stress (but not strain) jump when $\alpha \to 0$. This is consistent with the finding by Nemat-Nasser and Obata (1990) in which discontinuity is examined in an alternative manner.

It is interesting to note in Table 3 that an increase in crack speed can also enlarge the range of $(\mu - \beta)$. There should be an envelope similar to that in Fig. 3 for medium strain-hardening materials. Hence, increase of $(\mu - \beta)$ will set a lower limit to the crack speed. If the crack is lower than this limit, no solutions can be obtained due to the stress jump on the boundary of the elastic unloading sector and the secondary

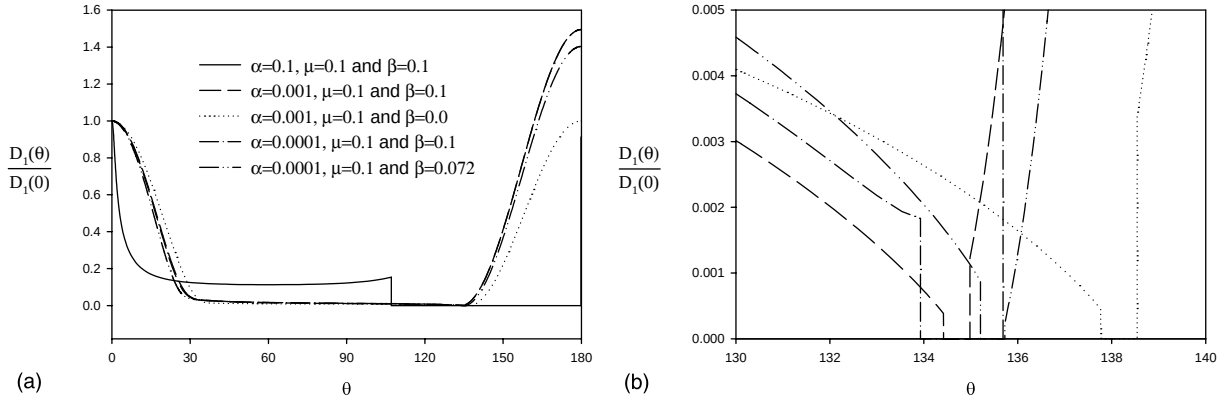

Fig. 13. (a) Angular distributions of normalized D_1 for various combinations of material parameters at $m_V = 0$. The elastic unloading zone is represented by the segment on the θ-axis by assuming $D_1 = 0$. (b) Enlarged portion of (a) between 130° and 140°.

plastic sector. However, at medium strain-hardening rates, the lower limit of the crack speed is determined by the occurrence of the singular behavior of the plastic potentials.

5. Discussion and conclusions

The motivation for the study of the effects of non-associativity on crack propagation comes from the fact that it is more suitable to some materials than the associated flow-rule. For example, the non-coaxial plastic behavior is not uncommon in geo-mechanics. Moreover, the inclusion of non-associativity produces more reasonable results on crack dynamics. Even though pressure-sensitivity reduces the singularity significantly compared with J_2-flow theory, stress singularity increases with increasing non-associativity degree. More importantly, it can be larger than those based on J_2-flow theory. It implies a further reduction in fracture toughness if the non-associativity is important at the later stage of material failure. Toughness reduction can be easily captured in experiments and numerical models by including the evolution of microstructures (see Wei, 2000 who considered the effects of microvoids). Although the non-associative plastic theory cannot be applied to describe the softening regime, it seems more reasonable than the associative pressure-sensitive models for the materials with plastic dilatation and deformation localization, like the nucleation and growth of small voids and microcracks.

As found by Li and Pan (1990) and Bigoni and Radi (1993) for associative plastic theories, the singular behavior of the plastic potential, that is, a hydrostatic state of stresses, can recur for non-associative cases. Material inertia can delay the occurrence of the singular behavior. However, we have not found such behavior at vanishing strain-hardening rates. The solutions at the upper limit of $(\mu - \beta)$ indicate a tendency to a discontinuity in the slope of radial stress $\hat{\sigma}_{rr}$ near the boundary of the elastic unloading region and the secondary plastic sector boundary. And the continuities in other stress components and velocities remain. It is shown from the perturbation analysis that the maximum non-normality degree depends much on the strain-hardening rate. The upper limit of $(\mu - \beta)$ is of the order $\alpha^{1/2}$.

Numerical results confirm again that material inertia plays an important role in stabilising crack growth by decreasing the singularity, whether plastic flow is associative or non-associative. It should be mentioned that the influence of crack speed on the strength of singularity depends strongly on α since it is a major factor in controlling the upper limit of the crack speeds in plane-strain. It is seen that the inertia effect can offset the destabilising effect of non-associativity in reducing the stress singularity. Especially when M_V

approaches unity, the inertia effect becomes more significant since the value of s can be reduced to one-tenth of that at $M_V = 0$ for $\alpha = 0.001$. But this does not mean that the increase in crack speed will definitely enhance the toughness. The dynamic fracture in ductile materials remains fully unexplored (see Rosakis and Ravichandran, 2000). This situation is caused by the coupled mechanism of complex material behavior and inertia. The lack of experimental tools makes it difficult to validate existing theories. From the results presented here, the variation of non-associativity with crack-tip speeds seems to provide a means to corroborate experimental measurements. Actually, the non-associativity changes with the extent of deformation (e.g., Rudnicki and Rice, 1975). It is expected that the non-associativity would become more important with increasing crack-tip speeds due to the evolution of microstructures. In this way, the increasing trend in toughness with increasing crack speed would be impossible at high crack speeds since non-associativity can destabilize crack growth. The competition between inertia effect and non-associativity could produce the phenomenon that cracks prefer to grow at a constant speed, as observed in experiments.

When M_V is increased to unity, there are kinks and a strong sign of slope discontinuity in shear stress and radial velocity at $\theta = \pi/2$ from the crack plane, for various combinations of material parameters. This is consistent with the numerical results of Varias and Shih (1994) for plane strain. The occurrence of slope discontinuity determines the crack speed limit M_V^L. It is found that M_V^L approaches unity at high and medium hardening rates, but it is lower than unity at vanishing hardening rates. Conversely, the lower limit of the crack speed can be determined by the singular behavior of the plastic potential at medium strain-hardening rates and by the discontinuity in the slope of angular distributions of radial stresses at vanishing hardening rates.

It has been argued that the upper crack speed limit is a material characteristic, as measured experimentally by Lee and Prakash (1998). However, the speed limit determined by the occurrence of jumps in near-tip fields seems to be much smaller than experimental observations. Two distinct reasons may contribute to this discrepancy. First, the asymptotic solutions can play a dominant role in the low strain-hardening materials. However, high strength structural steels are commonly used in dynamic fracture tests. Second, thin plate geometries are commonly used in dynamic fracture testing of ductile solids (see Mathur et al., 1996). The fracture process involves two distinct modes: plane strain conditions in the plate's interior and plane stress shear lips in the surface layers. Mathur et al. (1996) reported the initial tunneling crack surface and the subsequent shear-dominant crack extension. Although their competition at different loading rates remains elusive, the mode transition is evident in thin-plate impact tests. This phenomenon reveals that although crack initiation can be easily triggered in the interior, the crack growth speeds measured in the tests are mostly valid for plane stress. The limiting speed under plane strain should be much smaller than under plane stress, otherwise the initial tunneling shape would be the final crack surface because the fracture toughness in plane stress is higher than in plane strain. However, the limiting speed under plane stress conditions derived from asymptotic solutions is much higher than the plastic shear wave speed (see Zhang and Mai, 2000). It was argued by the authors that some important features of near-tip fields have not been captured by Hermann and Potthast (1995) for plane stress Mode I dynamic cracks in associative pressure-sensitive materials, because they used the plastic shear wave speed as the limiting speed. Some well-known fracture experiments on amorphous materials such as poly-methylmethacrylate by Ravi-Chandar and Knauss (1984) showed that the cracks did not propagate faster than about 0.4 and 0.5 of Rayleigh wave speed c_R. But recently, limit crack speeds up to 0.9 c_R, were observed in brittle crystalline materials (Cramer et al., 2000). Therefore, it is reasonable to conclude that the limiting crack speed varies with different materials.

The validation of the assumption of a sharp crack-tip is another issue for the asymptotic results. It depends on the size of the fracture process zone. Here we consider low strain-hardening materials. In these cases, a low stress singularity is found and the level of stresses ahead of the crack-tip is not high enough to cause intense material damage. The plastic zone would be much larger than the fracture process zone so

that the assumption of a sharp crack-tip is reasonable (see more details in Stahle, 1993). In addition, the non-associative material model is suitable for describing the evolution of microstructures to some extent, such as discussed by Tvergaard (1982) and Kuroda and Tvergaard (2001). Non-associativity can give approximations to what happens in the fracture process zone.

Acknowledgements

We wish to thank the Australian Research Council (ARC) for the continuing support of this project. X. Zhang was in receipt of an Overseas Postgraduate Research Award tenable at the University of Sydney and an ARC Research Scholarship when this work was carried out in the CAMT. Y.-W. Mai is Federation Fellow and Q.-H. Qin is Professorial Fellow both supported by the Australian Research Council.

Appendix A. The coefficients in matrix A and B in Eq. (11)

$$
\begin{aligned}
&a_{11} = 2\frac{c_V}{s}\sin^2\theta, \quad a_{13} = -1\\
&a_{22} = \frac{c_V}{s}\sin^2\theta, \quad a_{25} = -1\\
&a_{31} = -1, \quad a_{33} = s\left(1 + v + \frac{2}{h}Q_{r\theta}P_{r\theta}\right)\\
&a_{34} = \frac{s}{h}Q_{rr}P_{r\theta}, \quad a_{35} = \frac{s}{h}Q_{\theta\theta}P_{r\theta}, \quad a_{36} = \frac{s}{h}Q_{33}P_{r\theta}\\
&a_{43} = \frac{2}{h}Q_{r\theta}P_{rr}, \quad a_{44} = 1 + \frac{1}{h}Q_{rr}P_{rr}\\
&a_{45} = -v + \frac{1}{h}Q_{\theta\theta}P_{rr}, \quad a_{46} = -v + \frac{1}{h}Q_{33}P_{rr}\\
&a_{52} = -1, \quad a_{53} = \frac{2s}{h}Q_{r\theta}P_{\theta\theta}, \quad a_{54} = s\left(-v + \frac{1}{h}Q_{rr}P_{\theta\theta}\right)\\
&a_{55} = s\left(1 + \frac{1}{h}Q_{\theta\theta}P_{\theta\theta}\right), \quad a_{56} = s\left(-v + \frac{1}{h}Q_{33}P_{\theta\theta}\right)\\
&a_{63} = \frac{2}{h}Q_{r\theta}P_{33}, \quad a_{64} = -v + \frac{1}{h}Q_{rr}P_{33}\\
&a_{65} = -v + \frac{1}{h}Q_{\theta\theta}P_{33}, \quad a_{66} = 1 + \frac{1}{h}Q_{33}P_{33}\\
&b_1 = c_V\sin\theta\left(\cos\theta y_1 + \frac{\sin\theta}{s}y_2\right) + s(\cos\theta y_3 + \sin\theta y_4)\\
&b_2 = c_V\sin\theta\left(\cos\theta y_2 - \frac{\sin\theta}{s}y_1\right) + s(\cos\theta y_5 + \sin\theta y_3)\\
&b_3 = \frac{s-1}{2}y_2\\
&b_4 = y_1\\
&b_5 = y_1/s\\
&b_6 = 0
\end{aligned}
$$

in which $c_V = m_V^2/(2(1+v))$.

Appendix B. Quasi-static crack-tip fields

The solutions for the slip-line crack-tip fields in perfectly plastic materials are sought at a infinitesimal distance from the crack-tip. In the plastic sectors, the constitutive law can be written in the incremental form $\mathrm{d}\varepsilon_{ij}^{p} = \mathrm{d}\lambda P_{ij}$, in which $\mathrm{d}\lambda$ is a multiplication factor. In addition, the elastic response is isotropic and the elastic strain is incompressible. Under plane strain conditions, the out-of-plane deformation vanishes. Thus the requirement of $\varepsilon_{33} = 0$ becomes:

$$\sigma_{33} = \sigma - \frac{\beta}{\sqrt{1-\beta^2/3}}\tau \tag{B.1}$$

where $\sigma = (\sigma_{rr} + \sigma_{\theta\theta})/2$ and

$$\chi = \sqrt{\left(\frac{\sigma_{rr} - \sigma_{\theta\theta}}{2}\right)^2 + \sigma_{r\theta}}$$

Substituting (B.1) in the yield surface $f(\sigma) = \sigma_e/\sqrt{3} + \mu\sigma_{kk}/3 - \sigma_0 = 0$, it is rewritten as:

$$f = \frac{1-\mu\beta/3}{\sqrt{1-\beta^2/3}}\chi + \mu\sigma = \sigma_0 \tag{B.2}$$

where σ_0 is the yield stress in tension at vanishing strain hardening.

For simplicity, the equation can be rearranged as:

$$\chi = c - \sigma\tan\phi \tag{B.3}$$

in which

$$\begin{aligned} \sin\phi &= \frac{\mu\sqrt{1-\beta^2/3}}{1-\mu\beta/3} \\ c &= \sigma_0\left(\frac{1-\beta^2/3}{1-\mu^2-2\mu\beta/3+4\mu^2\beta^2/9}\right)^{1/2} \end{aligned} \tag{B.4}$$

As $r \to 0$, the equilibrium equations in the polar coordinate system are (Rice, 1982):

$$\begin{aligned} &\sigma_{rr} - \sigma_{\theta\theta} + \sigma'_{r\theta} = 0 \\ &2\sigma_{r\theta} + \sigma'_{\theta\theta} = 0 \end{aligned} \tag{B.5}$$

in which the prime denotes the derivative to the angle θ, i.e.,

$$\sigma'_{ij}(\theta) = \lim_{r\to 0}\left[\frac{\partial\sigma_{ij}(r,\theta)}{\partial\theta}\right]$$

The consistency condition, i.e., the use of the prime operator to (B.3), gives

$$Q_{ij}\sigma'_{ij} = 0 \tag{B.6}$$

An identity can be found in Rice (1982) for the calculation of the left term in (B.6). Let H_{ij} be an arbitrary tensor. Then from (B.5), the following expression for a planar problem is:

$$H_{ij}\sigma'_{ij} = (\sigma_{rr} + \sigma_{\theta\theta})'H_{rr} + \sigma'_{33}H_{33} \tag{B.7}$$

In the plastic sectors,

$$(\sigma_{rr}+\sigma_{\theta\theta})'Q_{rr}+\sigma'_{33}Q_{33}=0 \tag{B.8}$$

Furthermore, plane-strain constraint requires $P_{33}=0$ in plastic sectors since the plastic strain is defined by the flow potential. Thus:

$$Q_{33}=(\mu-\beta)/3 \tag{B.9}$$

Eliminating τ in (B.1) and (B.3), it provides:

$$\sigma'_{33}=\left(1+\frac{\mu\beta}{1-\mu\beta/3}\right)\sigma' \tag{B.10}$$

Substituting (B.9) and (B.10) in (B.8) gives:

$$(\sigma'_{rr}+\sigma'_{\theta\theta})\left(Q_{rr}+\frac{\mu-\beta}{6}\frac{1+2\mu\beta/3}{1-\mu\beta/3}\right)=0 \tag{B.11}$$

Thus, there are two forms of solutions for the stress fields in the plastic sectors: (i) constant stress sectors by $\sigma'_{rr}+\sigma'_{\theta\theta}=0$ and (ii) center fan sectors by

$$Q_{rr}=-\frac{\mu-\beta}{6}\frac{1+2\mu\beta/3}{1-\mu\beta/3}$$

However, for growing cracks, introduction of an elastic unloading zone between the primary plastic region and the plastic reloading region is very imperative, as pointed out by Rice (1982), for the elimination of negative plastic work across the elastic–plastic boundary.

References

Achenbach, J.D., Kanninien, M.F., Popelar, C.H., 1981. Crack tip fields for fast fracture of an elastic–plastic material. J. Mech. Phys. Solids 29, 211–225.

Amazigo, J., Hutchinson, J.W., 1977. Crack-tip fields in steady crack-growth with linear strain hardening. J. Mech. Phys. Solids 25, 81–97.

Bigoni, D., Radi, E., 1993. Mode I crack propagation in elastic–plastic pressure sensitive materials. Int. J. Solids Struct. 30, 899–919.

Brannon, R.M., Drugan, W.J., 1993. Influence of non-classical elastic–plastic constitutive features on shock wave existence and spectral solution. J. Mech. Phys. Solids 41, 297–330.

Cramer, T., Wanner, A., Gumbsch, P., 2000. Energy dissipation and path instabilities in dynamic fracture of silicon single crystal. Phys. Rev. Lett. 85, 788–791.

Gao, Y.C., Nemat-Nasser, S., 1983. Dynamic fields near a crack tip growing in elastic-perfectly-plastic solids. Mech. Mater. 2, 47–60.

Hermann, L.P., Potthast, B., 1995. Asymptotic crack tip fields for pressure-sensitive materials and dynamic crack growth under plane stress conditions. Int. J. Fract. 74, R53–61.

Kuroda, M., Tvergaard, V., 2001. A phenomenological plasticity model with non-normality effects representing observations in crystal plasticity. J. Mech. Phys. Solids 49, 1239–1263.

Lam, P.S., Freund, L.B., 1985. Analysis of dynamic growth of a tensile crack in an elastic–plastic material. J. Mech. Phys. Solids 33, 153–167.

Lee, Y., Prakash, V., 1998. Dynamic fracture toughness versus crack tip speed relationship at lower than room temperature for high strength 4340VAR structural steel. J. Mech. Phys. Solids 46, 1943–1967.

Leighton, J.L., Champion, C.R., Freund, L.B., 1987. Asymptotic analysis of steady dynamic crack growth in an elastic–plastic materials. J. Mech. Phys. Solids 35, 541–563.

Li, F.Z., Pan, J., 1990. Plane strain crack-tip fields for pressure-sensitive dilatant materials. J. Appl. Mech. 57, 40–49.

Lo, K.K., Peirce, D., 1981. Effect of yield surface vertex on crack-tip fields in mode III. J. Mech. Phys. Solids 29, 143–152.

Mandel, J., 1966. Contribution Theorique a l'Etude de l'Ecrouissage et des Lios de l'Ecoulement Plastique. In: Proc. 11th Int. Congr. Appl. Mech. Springer-Verlag, Berlin, p. 502.

Mathur, K.K., Needleman, A., Tvergaard, V., 1996. Three dimensional analysis of dynamic ductile crack growth in a thin plate. J. Mech. Phys. Solids 44, 439–464.

Mroz, Z., 1963. Non-associated flow laws in plasticity. J. Mech. II, 21–42.

Nemat-Nasser, S., Obata, M., 1990. Some basic issues in dynamic crack growth in elastic–plastic solids. Int. J. Fract. 42, 287–300.

Narasimhan, R., Rosakis, A.J., 1987. Reexamination of jumps across quasi-statically propagating surface under generalized plane stress in anisotropically hardening elastic–plastic solids. J. Appl. Mech. 54, 519–524.

Ostlund, S., Gudmundson, P., 1988. Asymptotic crack tip fields for dynamic fracture of linear-hardening solids. Int. J. Solids Struct. 24, 1141–1148.

Papanastasiou, P., Durban, D., 2001. Singular plastic fields in non-associative pressure sensitive solids. Int. J. Solids Struct. 38, 1539–1550.

Ponte-Castaneda, P., 1987. Asymptotic fields in steady crack growth in linear strain-hardening. J. Mech. Phys. Solids 35, 227–268.

Press, W.H., Flannery, B.P., Teukolsky, S.A., Vetterling, W.T., 1992. Numerical Recipes. Cambridge University Press, Cambridge.

Radi, E., Bigoni, D., 1992. Asymptotic fields of mode I steady-state crack propagation in non-associative elasto-plastic solids. Mech. Mater. 14, 239–251.

Ravi-Chandar, K., Knauss, W.G., 1984. An experimental investigation into dynamic fracture, III. On steady-state crack propagation and crack branching. Int. J. Fract. 26, 141–154.

Rice, J.R., 1982. Elastic–plastic crack growth. In: Hopkins, H.G., Sewell, M.J. (Eds.), Mechanics of Solids. Pergamon Press.

Rosakis, A.J., Ravichandran, G., 2000. Dynamic failure mechanics. Int. J. Solids Struct. 37, 331–348.

Rudnicki, J.W., Rice, J.R., 1975. Condition for the localization of deformation in pressure-sensitive dilatant materials. J. Mech. Phys. Solids 23, 371–394.

Spitzig, W.A., Sober, R.J., Richmond, O., 1976. The effect of hydrostatic pressure on the deformation behavior of maraging and HY 80 steels and its implications for plasticity theory. Metal. Trans. 7A, 1703–1710.

Stahle, P., 1993. Dynamic crack tip field at steady growth and vanishing strain-hardening. J. Mech. Phys. Solids 41, 919–936.

Tvergaard, V., 1982. Influence of void nucleation on ductile shear fracture at a free surface. J. Mech. Phys. Solids 30, 399–425.

Varias, A.G., Shih, C.F., 1994. Dynamic steady crack growth in elastic–plastic solids, Propagation of strong discontinuity. J. Mech. Phys. Solids 42, 1817–1848.

Wei, Y., 2000. Elastic–plastic crack advance under steady-state accompanied by the micro-void growth. Acta Mech. Sinica 32, 291–299 (in Chinese).

Zhang, X., Mai, Y.-W., 2000. Asymptotic fields for dynamic crack growth in pressure-sensitive elastic–plastic materials. Int. J. Solids Struct. 37, 6297–6319.